**Annales
Geophysicae**

The structure of flux transfer events recovered from Cluster data

H. Hasegawa[1], B. U. Ö. Sonnerup[2], C. J. Owen[3], B. Klecker[4], G. Paschmann[4], A. Balogh[5], and H. Rème[6]

[1]Institute of Space and Astronautical Science, Japan Aerospace Exploration Agency, Sagamihara, Kanagawa, Japan
[2]Thayer School of Engineering, Dartmouth College, Hanover, New Hampshire, USA
[3]Mullard Space Science Laboratory, University College London, Dorking, Surrey, UK
[4]Max-Planck-Institut für extraterrestrische Physik, Garching, Germany
[5]Space and Atmospheric Physics Group, Imperial College, London, UK
[6]Centre d'Etude Spatiale des Rayonnements, Toulouse, France

Abstract. The structure and formation mechanism of a total of five Flux Transfer Events (FTEs), encountered on the equatorward side of the northern cusp by the Cluster spacecraft, with separation of ∼5000 km, are studied by applying the Grad-Shafranov (GS) reconstruction technique to the events. The technique generates a magnetic field/plasma map of the FTE cross section, using combined magnetic field and plasma data from all four spacecraft, under the assumption that the structure is two-dimensional (2-D) and time-independent. The reconstructed FTEs consist of one or more magnetic flux ropes embedded in the magnetopause, suggesting that multiple X-line reconnection was involved in generating the observed FTEs. The dimension of the flux ropes in the direction normal to the magnetopause ranges from about 2000 km to more than $1\,R_E$. The orientation of the flux rope axis can be determined through optimization of the GS map, the result being consistent with those from various single-spacecraft methods. Thanks to this, the unambiguous presence of a strong core field is confirmed, providing evidence for component merging. The amount of magnetic flux contained within each flux rope is calculated from the map and, by dividing it by the time interval between the preceding FTE and the one reconstructed, a lower limit of the reconnection electric field during the creation of the flux rope can be estimated; the estimated value ranges from ∼0.11 to ∼0.26 mV m^{-1}, with an average of 0.19 mV m^{-1}. This can be translated to the reconnection rate of 0.038 to 0.074, with an average of 0.056. Based on the success of the 2-D model in recovering the observed FTEs, the length of the X-lines is estimated to be at least a few R_E.

Keywords. Magnetospheric physics (Magnetopause, cusp and boundary layers; Solar wind-magnetosphere interactions) – Space plasma physics (Magnetic reconnection)

Correspondence to: H. Hasegawa
(hase@stp.isas.jaxa.jp)

1 Introduction

A flux transfer event (FTE) (Russell and Elphic, 1978; Haerendel et al., 1978), observed by a spacecraft situated near the magnetopause, is characterized by a bipolar pulse in the magnetic field component, B_n, normal to the average magnetopause surface. FTEs have attracted much interest because they are thought to be a consequence of dynamical (time-dependent) magnetic field reconnection and to be an essential part of the solar wind-magnetosphere interaction. Several models have been put forward to explain the observed properties of FTEs, such as the bipolar signature in B_n and an enhancement of the field magnitude: (1) in the original interpretation by Russell and Elphic (1978), the signature is due to the passage of a bundle of reconnected flux tubes, produced by patchy and impulsive reconnection near the subsolar magnetopause. At least in the initial stage, the resulting flux tubes are strongly curved near the region where they cross the magnetopause. They are pulled generally poleward under the influence of magnetic tension and the magnetosheath flow. This poleward motion of the tubes along the magnetopause can explain the positive-to-negative (negative-to-positive) B_n perturbation seen in the northern (southern) hemisphere magnetosheath (e.g. Rijnbeek et al., 1984). (2) Lee and Fu (1985), on the other hand, suggested that the FTE signature may be associated with plasmoids or magnetic flux ropes formed between two or more reconnection X-lines that are active simultaneously and are roughly parallel to each other. (3) Southwood et al. (1988) and Scholer (1988) suggested that the FTE signature may result from an impulsive burst of reconnection along an extended X-line, without invoking a localization in local time of the reconnection process, as in the Russell-Elphic model. In this scenario, a temporal variation in the reconnection rate leads to the formation of a bulge in the magnetopause, which is observed by a spacecraft as the bulge propagates along the boundary into an unperturbed reconnection layer. (4) By contrast, the model

proposed by Sibeck (1990) does not even require reconnection to occur. Instead, it is proposed that a solar wind pressure pulse causes a traveling wrinkle in the magnetopause surface which causes the observed bipolar FTE signature.

In a recent global MHD simulation by Raeder (2006), the FTE formation involves both a multiple X-line formation and time dependence of the reconnection activity, but in a manner different from the above reconnection-based models: when the interplanetary magnetic field (IMF) is strongly southward, an X-line forms at low latitude and becomes active. In the presence of a significant tilt of the magnetic dipole in the GSM x–z plane, this X-line does not sit still but is swept poleward by the magnetosheath flow with the reconnection rate decreasing to nearly zero. A new X-line then forms near the location of the old X-line formation, the result being the creation of a flux rope between the old and new X-lines. Since this process repeats itself, this model accounts for the quasi-periodic occurrence of FTEs seen in observations (e.g. Rijnbeek et al., 1984). Raeder's results also indicate an exclusive preference for FTEs to occur in the winter hemisphere.

FTEs inherently involve 2-D or 3-D structures, thus their details may be studied by use of the Grad-Shafranov (GS) reconstruction technique, which can produce a cross-sectional map of space plasma structures under the assumption that they are approximately 2-D and time-independent. The technique was first developed by Sonnerup and Guo (1996), and Hau and Sonnerup (1999), for use with data from a single spacecraft. It was recently extended to ingest data from multi-spacecraft missions such as Cluster (Hasegawa et al., 2005). It has been successfully applied to encounters by spacecraft with magnetic flux ropes in the solar wind (Hu and Sonnerup, 2001, 2002; Hu et al., 2003) and with the magnetopause (Hu and Sonnerup, 2000, 2003; Hasegawa et al., 2004, 2005). Recently, GS reconstruction has been successfully applied to an FTE seen by Cluster (Sonnerup et al., 2004).

The GS method also allows us to discuss which of the above FTE models is plausible to explain observed FTE properties. The Russell-Elphic model inherently has a three-dimensional (3-D) aspect, since it involves creation of a bent magnetic flux tube. At first sight, the resulting flux tube may not seem suitable for GS reconstruction. But a local segment of the tube may well be sufficiently elongated in some direction to be approximated by a 2-D structure. Then its structure may be recovered by the technique, although the orientation of the flux tube would depend on the location of the observing spacecraft relative to the elbow of the flux tube. In fact, an FTE studied by Walthour et al. (1994) was analyzed using a 2-D model (Walthour et al., 1993), but was also interpreted by models that have a 3-D aspect in a global sense. The third FTE model (e.g. Southwood et al., 1988) involves bursty (time-dependent) reconnection and hence, in principle, the resulting time-evolving structure cannot be treated by the GS method. But once the structure has reached an

approximate equilibrium state, it may satisfy the GS model assumptions. The similar situation would apply to the second model (e.g. Lee and Fu, 1985), which requires simultaneous multiple X-line formation, and also to the FTEs seen in the Raeder's global MHD model. On the other hand, the pressure pulse model (Sibeck, 1990) can be verified or ruled out by simultaneous observation of FTEs from both sides of the magnetopause. Such an observation was in fact made by ISEE 1 and 2, when they were separated by a few thousand km (Farrugia et al., 1987). It confirmed that the observed FTE structure bulged out on both sides of the magnetopause, consistent with the reconnection-based models.

In the study reported here, the GS reconstruction technique is applied to a total of five FTEs identified by the four Cluster spacecraft when they were separated by about 5000 km. The purpose is to gain information about the FTE structure and behavior, such as its shape, size, orientation, motion, and magnetic topology. Based on the reconstruction results, we discuss the nature of the magnetopause reconnection process that led to the observed FTEs, such as the orientation, location, and length of X-lines. Implications for component and antiparallel merging are also discussed. Section 2 gives a brief description of the GS reconstruction technique. The results of the FTE reconstructions are shown in Sects. 3 and 4; the orientation of the FTE flux rope axis, determined by several different methods, is in Sect. 5; and our study is summarized in Sect. 6.

2 Method

The assumptions underlying the GS reconstruction are as follows: (1) the spatial gradient of the structure in some direction, z, which we refer to as the invariant axis, is much smaller than that in the other directions, x and y, perpendicular to the z direction, i.e. $\partial/\partial z \ll \partial/\partial x$, $\partial/\partial y$; (2) as seen in a frame moving with the structure, it is approximately time independent; (3) the structure is in an approximate magnetohydrostatic equilibrium, i.e. inertia effects are negligible. This is the case when the plasma velocities in the co-moving frame are sufficiently small compared to the Alfvén speed and the sound speed, and also, in the presence of higher plasma speeds, when the field-line (and hence the streamline) curvature and the variation of the field magnitude along field lines are small.

Under the above assumptions, the MHD force balance equation is reduced to $\boldsymbol{j} \times \boldsymbol{B} = \nabla p$, the equation describing the balance between magnetic tension and force from the gradient of total (magnetic plus plasma) pressure. It can be further reduced to the so-called Grad-Shafranov (GS) equation, in the x–y Cartesian coordinate system:

$$\frac{\partial^2 A}{\partial x^2} + \frac{\partial^2 A}{\partial y^2} = -\mu_0 \frac{dP_t}{dA}, \tag{1}$$

where A is the partial vector potential, $A(x, y)$, and P_t is the transverse pressure, $P_t = (p + B_z^2/(2\mu_0))$. The magnetic field is expressed by $\boldsymbol{B} = (\partial A/\partial y, -\partial A/\partial x, B_z(x, y))$. The field lines projected onto the reconstruction (x–y) plane are then represented as equi-A contour lines, and the axial field, B_z, as well as the plasma pressure, p, are functions of A alone. It follows that P_t and the axial current density, which is given by $j_z = dP_t(A)/dA$, are also functions of A alone. Because of this property, the right-hand side of the GS equation is known at all points along a field line (defined by a certain value of A), once P_t and its derivative dP_t/dA are known at one point on that field line. Since the observing spacecraft encounters many field lines as it traverses a structure, the right-hand side of the GS equation is known in the entire region of the x–y plane occupied by these field lines.

In general, the structure to be reconstructed is moving past the observing spacecraft. A proper frame of such a structure is the deHoffmann-Teller (HT) frame, in which the plasma flow is as nearly field-aligned as the velocity and magnetic field measurements permit. The frame velocity, V_{HT}, relative to the spacecraft can be determined by a least-squares procedure (e.g. Khrabrov and Sonnerup, 1998a).

Since time independence of the structure is assumed, temporal information obtained by a spacecraft can be converted to spatial information along the trajectory of the spacecraft moving through the structure. Consequently, all spatial information needed for the reconstruction becomes available at each point on the trajectory. When the HT velocity remains constant and hence the spacecraft trajectory relative to the moving structure is a straight line during the event, the values of A along the x axis, which is the projection of the spacecraft trajectory onto the x–y plane, can be calculated from the measured field component, B_y, by spatial integration,

$$A(x, 0) = \int_0^x \frac{\partial A}{\partial x}\, dx = -\int_0^x B_y(x, 0)\, dx. \tag{2}$$

The spatial integration can be transformed into time integration via the relation, $dx = -\boldsymbol{V}_{HT}\cdot\hat{\boldsymbol{x}}dt$ (see Hu and Sonnerup, 2003, and Hasegawa et al., 2004, for discussion of cases where the HT frame velocity is temporally varying). The outcome of the integration depends on the choice of the invariant (z) axis. In a single-spacecraft application, this choice is made by searching for an axis for which P_t becomes equal for any field line, defined by a specific A value that is encountered more than once along the spacecraft trajectory (Hu and Sonnerup, 2002). In the present study, which is based on multi-spacecraft measurements, we determine the axis in a different way (see below). The above integration allows us to determine $P_t(A)$ from plasma pressures and fields measured along the spacecraft trajectory, and thus to calculate the right-hand side of the GS equation in all regions of the x–y plane threaded by field lines crossing the trajectory. In other parts of the x–y plane, the field must be recovered via suitable extrapolations of the function $P_t(A)$.

Once the function $P_t(A)$ has been determined, the integration of the GS equation proceeds as follows: field components, B_x and B_y, measured at points along the trajectory are used as spatial initial values. New A and B_x values at grid points that are away from the x axis by small steps, $\pm\Delta y$, are calculated via the GS equation. The integration is continued until a 2-D map of $A(x, y)$, in the reconstruction domain is obtained. For details of the integration procedure, suppression of numerical instabilities, and validation against exact solutions of the GS equation, see Hau and Sonnerup (1999) and Hu and Sonnerup (2003). This single-spacecraft version of the GS method has also been validated by use of multi-spacecraft data (Hu and Sonnerup, 2000; Hasegawa et al., 2004).

Hasegawa et al. (2005) have developed a simple way to construct an optimal field map and to determine the invariant axis by use of data from all four Cluster spacecraft. It proceeds in the following steps: (1) determination of a joint HT frame is made by combining Cluster 1 (C1) and C3 measurements of the velocity by the CIS/HIA instrument (Rème et al., 2001) and of the magnetic field by the FGM instrument (Balogh et al., 2001) (C2 and C4 lack CIS/HIA measurements). (2) When electron density data are available from the EFW instrument (Gustafsson et al., 2001), the plasma pressure, required for the reconstruction, is estimated not only for C1 and C3 but also for C2 and C4, via a relationship, established from C1 and C3 data, between the pressure and the electron density. (3) Choice of a joint trial invariant axis is made. This establishes a joint reconstruction coordinate system, allowing determination of functions $P_t(A)$ and $B_z(A)$ that are common to all four spacecraft. (4) Four magnetic field maps are produced, one for each spacecraft. In each map, the magnetic field measurements by one spacecraft are used to initiate the GS integration. (5) In each map, the A value at each grid point is weighted by a Gaussian function of y, which has its maximum at the y-value of the spacecraft trajectory. The four weighted A values are then added at each point of a joint grid, the result being a combined map of A, i.e. of the magnetic field projected onto the x–y plane. The map of $B_z(x, y)$ is based on the joint function $B_z(A)$. (6) The correlation coefficient between the three field components predicted by the composite map along each of the four spacecraft trajectories and the corresponding actually measured field components is calculated. It is then optimized, by trial and error, by varying the choice of the invariant axis, the needed extrapolation of the functions, $P_t(A)$ and $B_z(A)$, and the width of the Gaussian weight function. The optimal map and invariant axis result only after a large number (more than one hundred) of trial reconstructions have been performed. The optimal map no longer obeys the GS equation precisely but preserves $\partial/\partial z=0$ and $\nabla\cdot\boldsymbol{B}=0$. It accommodates deviations from the model assumptions, for example, it may incorporate inertia effects to some extent (Hasegawa et al., 2005). Once the optimum has been found, one can also produce maps showing the plasma pressure, p, number
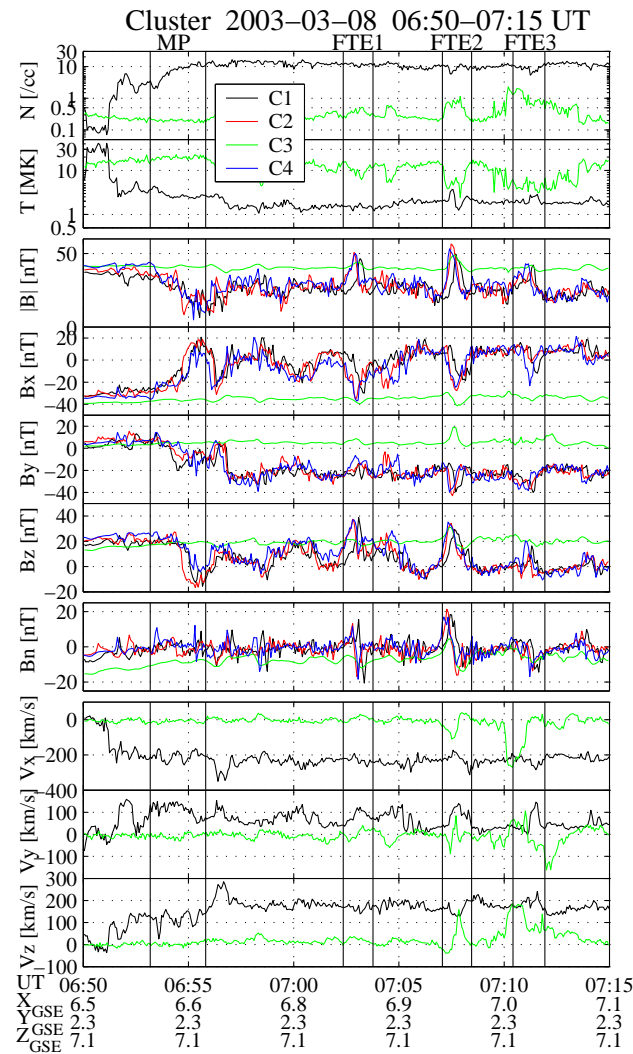
Fig. 1. Cluster data on 8 March 2003, 06:50–07:15 UT. The panels, from top to bottom, show: number density, ion temperature, magnitude and GSE components of the magnetic field, field component normal to the magnetopause, and GSE velocity components. The GSE location of Cluster was approximately $(6.9, 2.3, 7.1)\,R_E$. Time interval between the first pair of vertical lines was used for determining the normal to the magnetopause from the minimum variance analysis of the magnetic field (MVAB) measured by the Cluster 1 spacecraft (C1). The following three intervals, each including one flux transfer event, were used for the reconstruction.

density, N, and temperature, T, by determining optimal functions $p(A)$, $N(A)$, and $T(A)$, the assumption being that N and T are both constant along any field line, i.e. are functions of A alone. The current density in the reconstruction plane, j_t, is parallel to the transverse field lines and is given by $j_t = (1/\mu_0)(dB_z/dA)\boldsymbol{B}_t$, where $\boldsymbol{B}_t = (B_x, B_y)$. In the present paper, only the field and pressure maps will be presented but the axial current associated with FTEs will also be discussed.

3 Cluster event on 8 March 2003

3.1 Background information

Figure 1 shows an overview of the plasma and magnetic field measurements by Cluster for the period 06:50–07:15 UT on 8 March 2003. The spacecraft separation was about 5000 km. At the start of the interval, all four spacecraft resided in the dayside magnetosphere equatorward of the northern cusp. Three of the spacecraft, Cluster 1 (C1), C2, and C4, then crossed the magnetopause at ~06:55 UT and exited into the magnetosheath, as is clear from changes in the direction and intensity of the magnetic field. But C3 remained in the magnetosphere throughout the interval. Five FTEs occurred consecutively at ~06:58 UT, ~07:03 UT, ~07:07 UT, ~07:11 UT, and ~07:14 UT, as seen from the field magnitude enhancement and positive-then-negative B_n perturbation (3rd and 7th panels of Fig. 1). They appeared quasi-periodically with a period of 4–5 min, roughly consistent with a mean period of 8 min found in the ISEE events (e.g. Rijnbeek et al., 1984). In the present study, three prominent FTEs, marked as FTEs 1–3 in the figure, will be reconstructed and studied in detail, since at least one of the spacecraft saw substantial field perturbations and appears to have penetrated into the core portion of each FTE. For these FTEs, electron density data were not available from the EFW instrument. Therefore, the plasma pressure, needed to determine $P_t(A)$, was calculated solely from the CIS/HIA measurements on board C1 and C3. For each FTE, the interval sandwiched between a pair of vertical lines in Fig. 1 is used in the reconstruction. The magnetopause interval (06:53:11–06:55:49 UT) is also shown in the figure.

3.2 FTE 2

We first revisit FTE 2, which has already been studied by Sonnerup et al. (2004). The HT frame velocity, $\boldsymbol{V}_{HT}$, calculated from the combined C1 and C3 data, is $(-234, 51, 166)$ km s^{-1} in GSE, indicating that the structure was moving mainly anti-sunward and northward. The correlation coefficient between the GSE components of $\boldsymbol{v} \times \boldsymbol{B}$ ($\boldsymbol{v}$ denotes measured velocity) and the corresponding components of $\boldsymbol{V}_{HT} \times \boldsymbol{B}$ is cc$_{HT}$=0.938, and the slope of the regression line in the Walén plot of the combined C1 and C3 data (in which GSE velocity components, transformed to the HT frame, are plotted against the corresponding components of the local Alfvén velocities), hereafter referred to as the Walén slope, is -0.16. The latter means that the flow speed in the HT frame was small relative to the Alfvén speed, indicating that no active local reconnection was occurring at the time of the FTE encounter. In the present study, the Walén slope is always derived from the combined C1 and C3 data.

Figure 2, which was not shown by Sonnerup et al. (2004), shows the transverse pressure P_t and axial magnetic field B_z, as functions of A, for an optimal choice of the invariant (z)
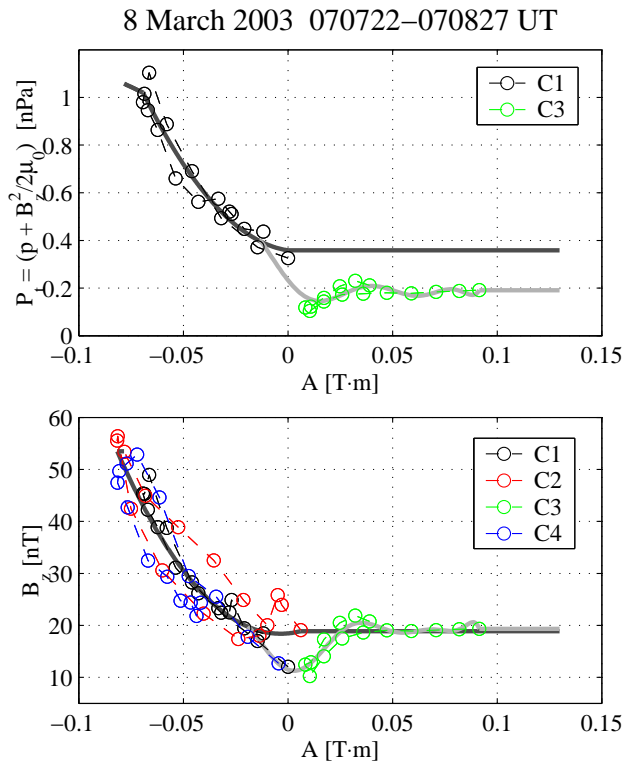
8 March 2003 070722–070827 UT

Composite Map, 8 Mar. 2003 070722–070827 UT

Fig. 2. Transverse pressure $P_t = (p + B_z^2/(2\mu_0))$ (top) and axial magnetic field component B_z (bottom) versus partial magnetic vector potential A for FTE 2. The fitted curves are polynomial functions of A; $P_t(A)$ is determined using the data points from C1 and C3 for which the CIS/HIA and FGM instruments were both operative, while $B_z(A)$ is determined using those from all four spacecraft. The black branch of the curves is used for reconstructing the magnetic flux rope and magnetosheath region (seen in the upper part of the maps in Fig. 3), while the gray branch is for the magnetospheric region (lower part).

axis orientation, $z = (-0.3296, -0.7434, 0.5820)$ (GSE). B_z values from different spacecraft are similar at a fixed A value, as they should be when the structure is approximately 2-D and magnetohydrostatic. The left part of the figure, where the fitted curves have only one branch, corresponds to the core part of the FTE, while the right part corresponds to the regions away from the FTE core, where there is a magnetospheric and a magnetosheath branch. It is the slope of the curve, $dP_t(A)/dA$, representing the axial current, that determines the structural characteristic of the FTE. The extrapolated lines on the right side are simply taken to be horizontal (no axial current); they have no significant influence on the reconstructed structure. The bottom panel shows that the data points from C2 and C4 reach a smaller A value (~ -0.08 Tm) than the C1 data points. This suggests that C2 and C4 were the closest to the center of the FTE structure at their closest approach, consistent with what can be seen from the optimal map, which is shown in Fig. 3.
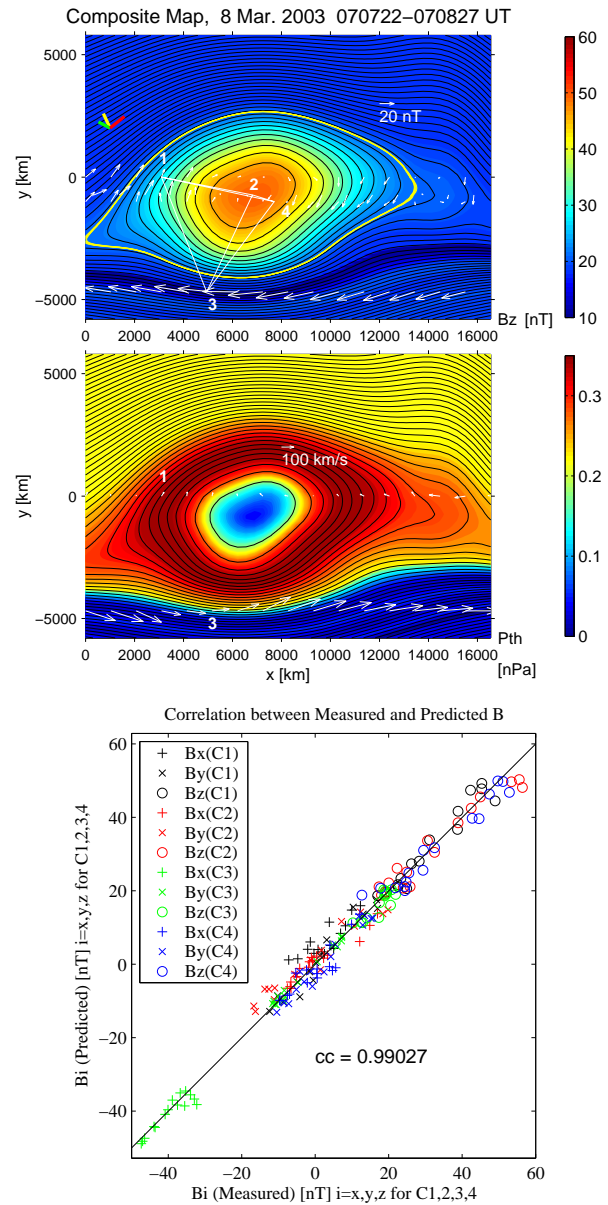
Fig. 3. The top two panels show magnetic field and pressure maps for FTE 2. Reconstructed field lines (in black) are projected onto the plane perpendicular to the invariant (z) axis, with axial field (top panel) or plasma pressure (second panel) in color. In the top panel, Cluster tetrahedron and measured transverse field, $B_t = (B_x, B_y)$ are shown in white. Colored line segments in the upper-left part are GSE unit vectors, X (red), Y (green), and Z (yellow), projected onto the x–y plane. In the middle panel, white arrows represent measured transverse velocity, transformed into the deHoffmann-Teller frame. The equatorward edge of the map is to the right, with the magnetosphere on the bottom. The bottom panel shows magnetic field components along reconstruction coordinates axes (x, y, z), predicted from the field map, versus those actually measured along the four spacecraft trajectories.
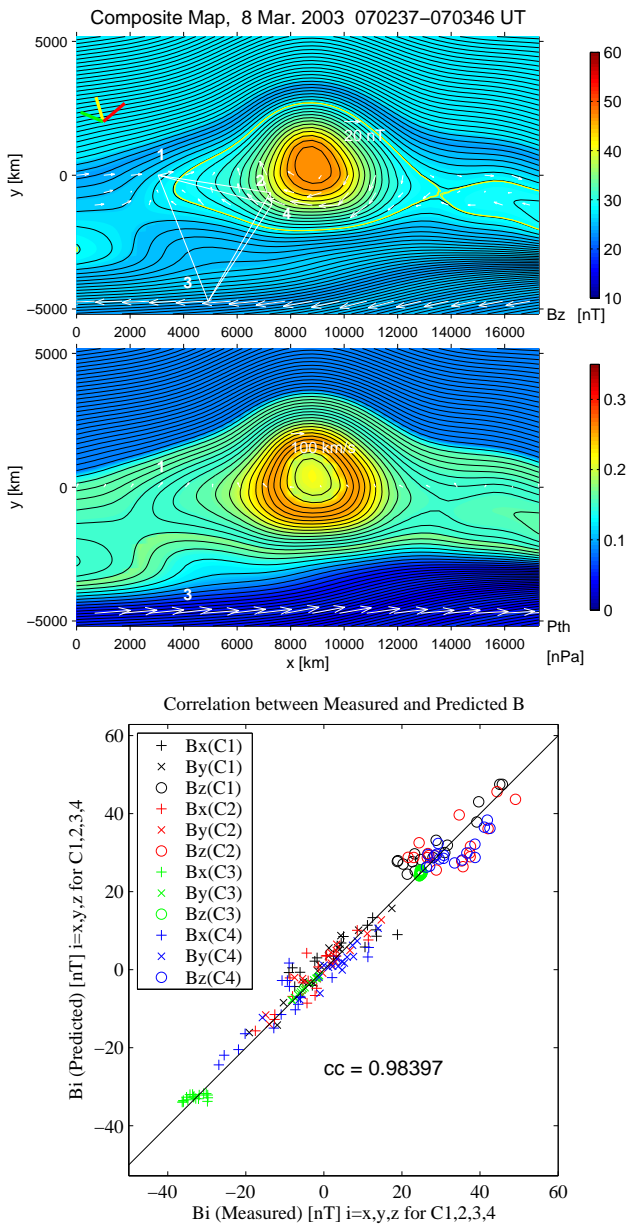
Composite Map, 8 Mar. 2003 070237–070346 UT

Correlation between Measured and Predicted B

Fig. 4. Field and pressure maps and associated scatter plot for FTE 1. The format is the same as in Fig. 3.

The top panel in Fig. 3 shows the optimal field map in which magnetic field lines in the x–y plane are shown by black curves and the axial (z) field component by colors. In this map, the equatorward side, where the observed FTE was presumably generated, is to the right and the poleward side to the left. Also, the magnetosphere is in the lower part and the magnetosheath is in the upper part of the map. This arrangement is used in all maps shown in this paper. The Cluster spacecraft were moving to the right in the frame of the map, that is, the structures were advected to the left in

the spacecraft rest frame. White arrows, with their tails anchored to points along the four spacecraft trajectories, represent measured transverse fields. These are nearly perfectly aligned with the reconstructed field lines and, indeed, the correlation coefficient between the three components of the magnetic field measured by the four spacecraft and the corresponding components predicted from the map is very high (cc=0.9903), as shown in the bottom panel of Fig. 3.

A prominent magnetic flux rope is seen in the map. The flux rope cross section is roughly circular but is somewhat elongated along the magnetopause. The axial field, B_z, shown in color, is stronger close to the center of the flux rope. The yellow field-line loop in the map contains a transverse magnetic flux per unit length along the z axis of 0.0518 Tm, an axial magnetic flux of 1.96×10^6 Tm^2, and an axial current of -0.64×10^6 A. The size of the flux rope along the normal to the magnetopause is $\sim 1\,R_E$, consistent with the dimension estimated long ago from the coordinated observations by the ISEE 1 and 2 spacecraft (Saunders et al., 1984). The yellow loop also shows that the FTE bulge is somewhat larger on the magnetosheath side than on the magnetosphere side.

The middle panel in Fig. 3 shows a color map of the thermal pressure. The white arrows in this map represent transverse velocities, $v_t' = (v - V_{HT})_t$, seen in the HT frame. These arrows are larger in the magnetosphere, while they are much smaller in the magnetosheath, indicating that the HT frame, i.e. the flux rope, was moving approximately with the magnetosheath plasma. No high-speed flow is seen within the flux rope, meaning that no signature of active local reconnection was present. The velocity arrows should, strictly speaking, be precisely parallel to the magnetic field lines. In reality there are deviations from this behavior, indicating the presence of some time variations. The pressure is seen to be enhanced in a ring-shaped region around the center of the flux rope, but interestingly has a minimum at the center, an interpretation of which has been discussed by Sonnerup et al. (2004).

3.3 FTE 1

The top panel in Fig. 4 shows the optimal field and pressure map for FTE 1, which occurred prior to FTE 2. The HT frame is fairly well determined with an HT velocity of $(-256, 62, 168)$ km s^{-1} in GSE, and cc$_{HT}$=0.976. The Walén slope is very small (-0.09), suggesting that no local reconnection-associated flow was present. The optimal invariant (z) axis is determined to be $(-0.4732, -0.6430, 0.6021)$ in GSE. For this axis orientation, the correlation coefficient between the measured and predicted magnetic field components is 0.9840, as shown in the bottom panel of Fig. 4. This is somewhat lower than that for FTE 2, but still very high, lending credence to the accuracy of the map. A prominent flux rope is seen but is somewhat smaller in size than FTE 2. It is also evident, as in FTE 2, that the flux rope bulge is much larger on the magnetosheath side than on the

magnetospheric side and that the core field component, along the flux rope axis, is strong. The total circumferential transverse magnetic flux per unit length, axial magnetic flux, and axial current, inside the yellow field-line loop are 0.045 Tm, 1.05×10^6 Tm^2, and -0.39×10^6 A, respectively. An X-point is embedded in the magnetopause on the poleward and on the equatorward side of the flux rope, suggesting that multiple X-line reconnection was involved in its creation. The bottom map of Fig. 4 shows that the pressure is again enhanced in a ring around the core of the flux rope, but the reduction at the center is not as strong as in FTE 2. As for FTE 2, the velocity, seen in the HT frame, is very small on the magnetosheath side, meaning that the flux rope was well anchored to the magnetosheath plasma.

3.4 FTE 3

For this FTE, the GSE components of the HT velocity are $(-249, 35, 205)$ km s^{-1} and cc$_{HT}$=0.976, indicating the presence of a good HT frame. The Walén slope is -0.08, meaning that there were no significant field-aligned flows at the location of the spacecraft. The maps in Fig. 5 show the optimal field and pressure maps for an optimal invariant axis, $z=(-0.4333, -0.7720, 0.4650)$ (GSE). As seen in the bottom panel, there is a good correlation (cc=9869) between the measured and predicted magnetic field components, indicative of the accuracy of the map. A pronounced flux rope, again having a strong core field, is present with its center at $(x, y)=(11\,000, -1500)$ km, although its size is about one-half of that in FTE 1. A second, more elongated flux rope is embedded in the magnetopause on the left (poleward) side of the primary flux rope, although the presence of the two FTE bulges cannot be seen the time plot (Fig. 1). The two bulges are separated by an X-point located at $(x, y) \sim (8000, -1000)$ km. Since none of the spacecraft crossed the smaller, flattened flux rope on the left, we cannot discuss the details of its internal structure, but since curved field lines were remotely sensed by the spacecraft, the presence of the structure itself should not be doubted. Unlike FTEs 1 and 2, the plasma pressure in FTE 3 appears to be reduced below the magnetosheath values throughout the main flux rope. But its actual behavior near the center of the flux rope remains unknown since none of the spacecraft actually sampled this region. The velocities seen by C1, transformed to the HT frame, are generally small, but are somewhat enhanced when C1 was near to, but somewhat to the right of, the main flux rope. This enhancement may possibly indicate that C1 detected flows associated with reconnection that occurred on the right (equatorward) side of the flux rope. Although the Walén slope is small, Fig. 1 shows that V_z is appreciably enhanced relative to its magnetosheath value during this interval. The spacecraft C3 observed dense (>1 cm^{-3}) ions with a magnetosheath-like velocity at the start of the interval (along the orbit in the left region of the map), while later on it detected low-density, magnetospheric ions. This indicates
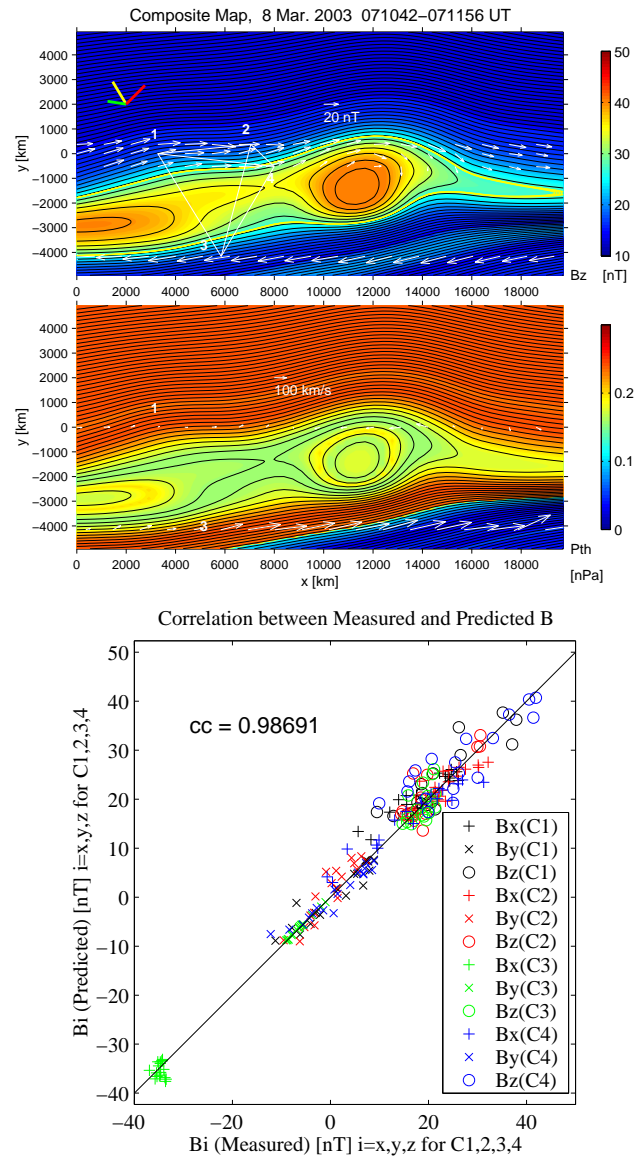

Fig. 5. Field and pressure maps and associated scatter plot for FTE 3.

that C3 was initially in a boundary layer present earthward of the magnetopause, and then moved into the magnetosphere proper. This behavior is consistent with what is shown by the map.

4 Cluster event on 26 January 2003

4.1 Background information

The two FTEs discussed in the following subsections occurred equatorward of the northern cusp, as in FTEs 1–3, but further duskward. Figure 6 shows Cluster data for 20:49–
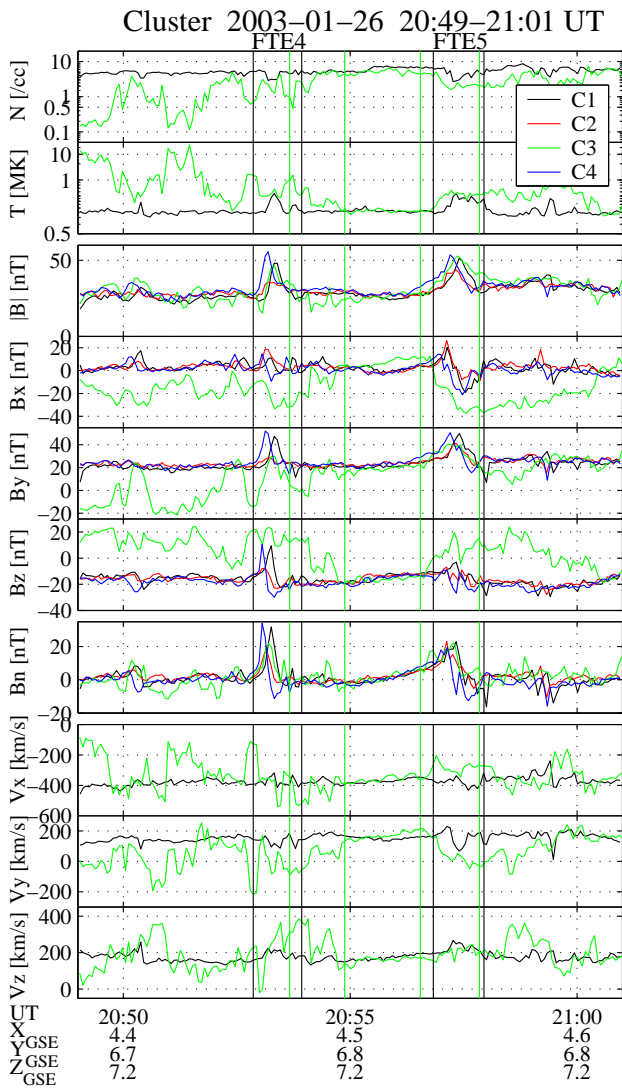
Fig. 6. Cluster data on 26 January 2003, 20:49–2:101 UT. The format is the same as in Fig. 1. The average GSE location of Cluster was $(4.5, 6.8, 7.2) R_E$. Time intervals between the black vertical lines were used for the FTE reconstruction, while those between the green vertical lines were for determining the magnetopause normal for FTEs 4 and 5, respectively, from MVAB with constraint $\langle B_n \rangle = 0$, using C3 magnetic field measurements.

Fig. 7. Field and pressure maps and associated scatter plot for FTE 4.

21:01 UT on 26 January 2003, during which the two FTEs, called FTEs 4 and 5, were identified. For these FTEs, positive-then-negative B_n perturbation, typical of FTEs seen in the Northern Hemisphere, and the usual field intensification, were observed. Three of the spacecraft, C1, C2, and C4, were mostly in the magnetosheath, while C3 was skimming the magnetopause, sometimes crossing the boundary, for example, at ~20:54 and ~20:57 UT. The measured magnetic field and plasma density from C3 were highly perturbed, switching between the magnetosheath and magnetospheric values. Intermittent and substantial increases in V_z were
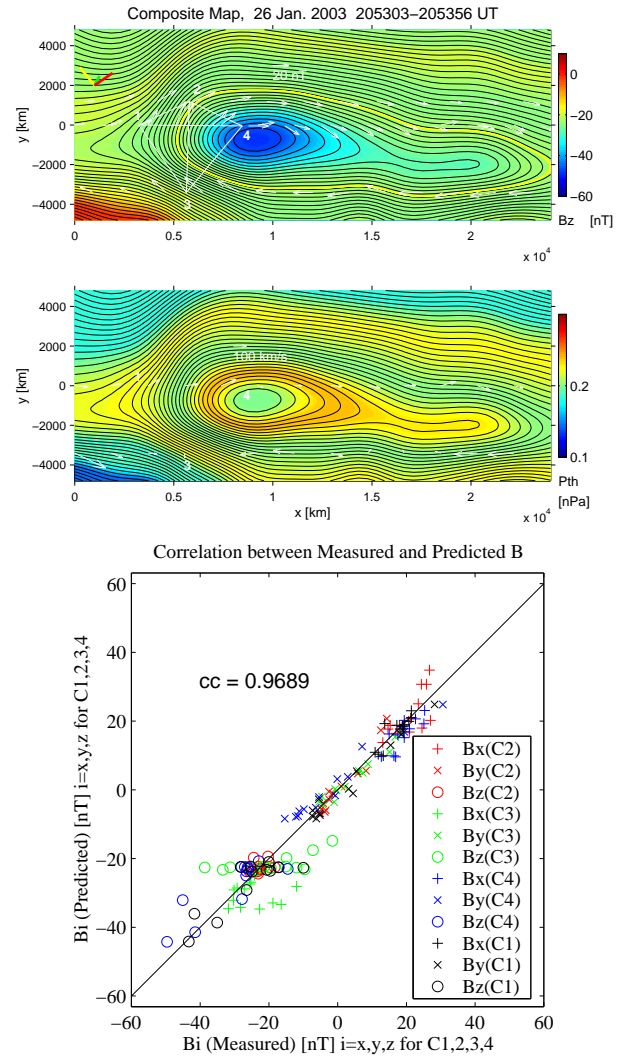
seen, presumably because of reconnection that was occurring at lower latitudes. The plasma density observed inside the magnetopause was often intermediate between the magnetosheath and magnetospheric values (>0.5 but $<4.0\,\mathrm{cm}^{-3}$), suggesting that C3 was in a boundary layer for a significant fraction of the time. For FTEs 4 and 5, the electron density data from EFW are available and were used for estimating the plasma pressure at C2 and C4, for which plasma measurements from CIS/HIA are not available.

4.2 FTE 4

We apply the GS method to the interval 20:53:03–20:53:56 UT during which FTE 4 occurred. The HT velocity for this interval is $(-386.7, -12.2, 267.6)\,\mathrm{km\,s}^{-1}$, with $\mathrm{cc}_{HT}=0.9696$. This indicates that this FTE was mainly

moving anti-sunward, northward, and, interestingly, weakly dawnward, despite the fact that Cluster was substantially duskward of the noon-midnight meridian. The Walén slope is significantly positive (0.3894), with a correlation coefficient in the Walén plot of 0.8356, implying the possibility of some ongoing local reconnection activity. The map for this event (Fig. 7) shows a magnetic flux rope that is strongly elongated in the direction tangential to the magnetopause. As shown in the scatter plot, the correlation coefficient between the measured and predicted field components is 0.9689, for an optimal choice of the invariant axis, z=(0.4055, −0.8945, 0.1884), indicating that the GS method works fairly well. As in the previous FTEs, the flux rope has a strong core field and plasma pressure enhancement in a ring around its center. The transverse magnetic flux, axial magnetic flux, and axial current, contained within the yellow loop, are 0.0619 Tm, -1.92×10^6 Tm^2, and -0.63×10^6 A, respectively. The pressure map shows that, contrary to the previous FTEs, the magnetosheath plasma (with velocities measured by C1 and transformed to the HT frame) was streaming parallel to the magnetic field lines at a substantial speed. This field-aligned flow leads to the significantly positive Walén slope and to the entry of magnetosheath plasmas into the magnetosphere, as a result of the magnetosheath field lines being connected to the magnetospheric side. This feature, as well as the flatness of the flux rope shape, implies that, at the time of observation, reconnection was going on, and that the flux rope had not yet reached an equilibrium: it was still temporally evolving toward a final, more rounded cross section. This interpretation explains why the correlation between the measured and predicted magnetic fields (the bottom panel of Fig. 7) is less good than in the previous FTEs. The lower correlation is indicative of some breakdown of the model assumptions. The minor dawnward component of the HT velocity can be explained by still active reconnection that would accelerate the plasma dawnward for the observed magnetosheath field condition ($B_y>0$), on the northern side of an X-line. Note that, as shown in Table 2, the HT velocity component perpendicular to the invariant axis is somewhat larger for FTE 4 than for FTE 5 (discussed below). This is consistent with the plasma acceleration due to reconnection that is present in FTE 4 but not in FTE 5. The latter FTE had no reconnection signatures and was well anchored in the magnetosheath plasma (see Fig. 8).

Examination of ion distribution functions seen by C3 shows the presence of two distinct magnetosheath-like ion populations, streaming in the field-aligned, but opposite, directions in the HT frame. In addition, the two populations were occasionally D-shaped, i.e. had a cutoff in the distributions at a certain field-aligned velocity (e.g. Cowley, 1982). These features may be associated with the above-mentioned reconnection activity: they appear consistent with the interpretation that two X-lines were present, as inferred from the map, and that the two populations came from the X-line on each side of the primary flux rope.

4.3 FTE 5

This FTE occurred about 4 min later than FTE 4. For the interval 20:57:00–20:57:57 UT, the HT velocity is (−377, 94, 240) km s^{-1}, with cc$_{HT}$=0.974. No significant field-aligned velocity was present at either C1 or C3; the Walén slope based on the combined C1 and C3 data is 0.12. The optimal field map for FTE 5 in Fig. 8 indicates that a fairly large flux rope was present. The size of the whole flux rope structure in the normal direction is comparable to, or somewhat larger than, that of FTE 2. The elongation of the flux rope in the tangential direction is more pronounced than in FTEs 1 and 2, implying that this flux rope was still in a phase of deformation. For an optimal invariant axis orientation of (0.3639, −0.9145, 0.1768) (GSE), the measured and predicted magnetic field variations have a good correlation (cc=0.9794), indicating the accuracy of the map. As in all of the other flux ropes, the axial field and plasma pressure are intense in a region around the center. However, the center region itself was not encountered by any of the four spacecraft, so that the slight depression of the plasma pressure, shown in Fig. 8 near the center itself, is the result of extrapolation of the function $p(A)$ and may not be real. The transverse magnetic flux, axial magnetic flux, and axial current, inside the yellow loop, are 0.0621 Tm, -3.59×10^6 Tm^2, and -0.70×10^6 A, respectively. As in FTEs 1 and 2, the FTE bulge is larger on the magnetosheath side than on the magnetosphere side. The velocity in the HT frame is negligible on the magnetosheath side, meaning that the flux rope was well anchored to the magnetosheath plasma.

5 Orientation of flux rope axis

We now compare the orientation of the invariant (z) axis determined from optimal GS reconstruction with those from various single-spacecraft methods. We also examine the relation of the axis orientation to the direction of the magnetosheath magnetic field, the objective being to infer the geometry of magnetopause reconnection that led to the FTEs. Polar plots for the five FTEs are shown in Fig. 9. In these diagrams the directions of the flux rope axes from several methods are plotted. The bull's-eye represents the vector $n\times(k\times n)$, where n is the magnetopause normal from the minimum variance analysis of the magnetic field (MVAB) for the intervals denoted in Figs. 1 and 6, and k is the orientation of the invariant axis from optimal GS reconstruction. The normal for FTEs 1–3 is determined based on C1 data to be (0.6444, 0.2446, 0.7245) (GSE), with the intermediate to minimum eigenvalue ratio of 8.6. From this ratio, the angular uncertainty of the normal is estimated to be ∼3.5° based on Eq. (8.23) in Sonnerup and Scheible (1998). As for FTEs 4 and 5, the intermediate to minimum eigenvalue ratio is 3.3 (based on C3 data for the interval 20:53:40–20:54:53 UT) and 1.6 (for 20:56:33–20:57:51 UT), respectively, indicating
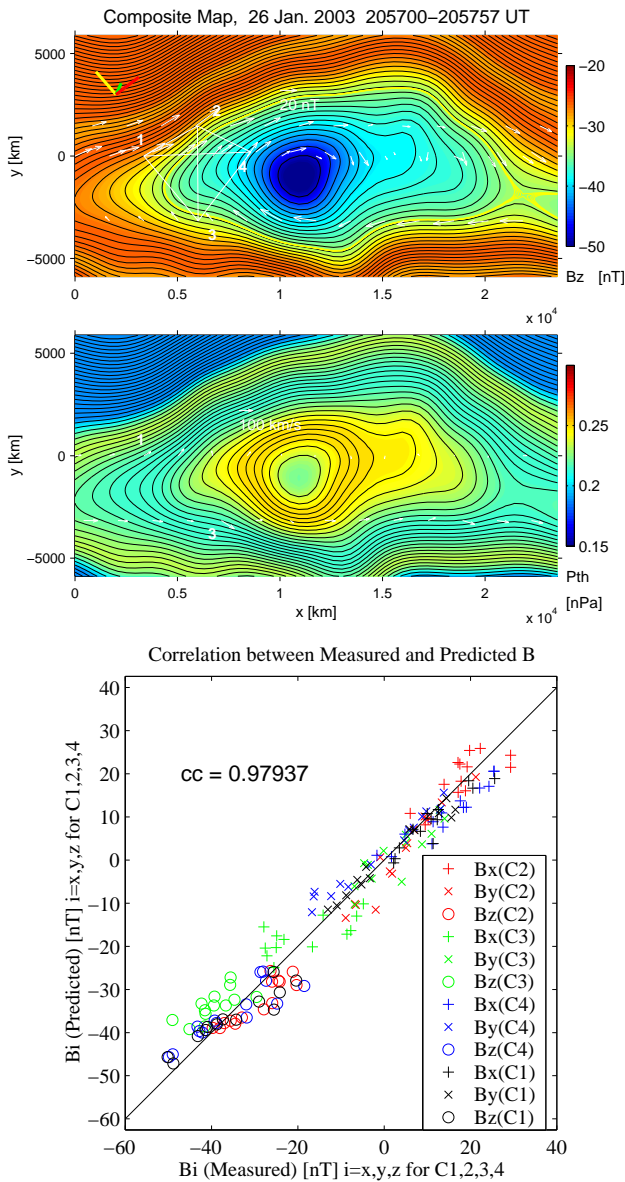
Fig. 8. Field and pressure maps and associated scatter plot for FTE 5.

a large uncertainty in the normal. Therefore, we determine the normal with constraint $\langle B_n \rangle = 0$ (MVABC), the result being (0.4534, 0.5151, 0.7274) for FTE 4 and (0.3964, 0.1180, 0.9105) for FTE 5. It must be kept in mind, however, that even these normals may not be accurate, because the two intervals somewhat coincide with the corresponding FTE, which is found to have a significant 2-D structure, and the two normals have a substantial angle (∼25°) to each other. Here the normals are used simply to define a reasonable coordinate system for the polar plots.

The GS axis is marked by a white dot, along with white contour lines on which the correlation coefficient between

the measured and predicted field components (see, for example, the bottom panel of Fig. 3) is equal. The interval between the neighboring contour lines represents the correlation coefficient difference of 0.001. It is seen that, except for FTE 4, the contour lines are elongated horizontally in the polar plots, i.e. in the direction perpendicular to the magnetopause normal. This indicates that the axis is less accurately determined for rotation about the normal vector, consistent with the result obtained by Hasegawa et al. (2004). It may be worth noting that one magnetopause event, identified by Cluster on 5 July 2001, and studied by Hasegawa et al. (2004), also did not show the horizontal elongation of the angle domain having high correlations (see their Fig. 15). In this event there was substantial reconnection activity, even more so than in FTE 4. It may be that the correlation coefficient becomes more sensitive to the rotation of the invariant axis about the normal direction when significant reconnection activity is present. For FTEs 1 and 2, the GS axis is perpendicular to the magnetopause normal within the range of uncertainty, as expected. For FTEs 3–5, the angular scale in the polar plots is more coarse and the perpendicular condition is less well satisfied. It is likely that the orientation of the magnetopause normal at the time FTE 3 was encountered tipped by about 8° from that observed near 06:55 UT. Furthermore, in particular for FTE 5, where the deviation from the perpendicular condition is the largest (slightly more than 10°), the normal may not be accurately determined since, as Fig. 6 shows, the interval to which MVAB has been applied nearly coincides with that of the FTE. This interval, therefore, contains outstanding 2-D structures, leading to a violation of the one-dimensional assumption that forms the basis of MVAB. Therefore, it is not easy for FTEs 3–5 to conclude whether the flux rope was lying flat on the magnetopause or was sticking into the magnetosphere/magnetosheath at a finite angle. We cannot exclude the possibility, as expected in the Russell-Elphic model, that it was penetrating into/out of the magnetosphere.

We now turn to the various single-spacecraft determinations of the axis orientation. Hu and Sonnerup (2002) determined the invariant axis in such a manner that the transverse pressure, P_t, became as nearly equal as their data permitted, at certain A values for which more than one data point was available. This method is based on the condition that, in a magnetohydrostatic equilibrium, P_t and B_z should be constant on a field line. In Fig. 9, the axis thus determined is marked by the orange asterisk, and the background colors show a map of a residue associated with the fitting of $B_z(A)$, as defined by Eq. (5) in Hu and Sonnerup (2002). The residue is computed using the data from C1, which approached the flux rope center more than C3. We used the axial field B_z, not the transverse pressure P_t, to compute the residue, since the measurements of the magnetic field are, in general, more accurate than those of pressure. The residue reaches zero when B_z values measured at different times are precisely equal over a range of A in which more than one
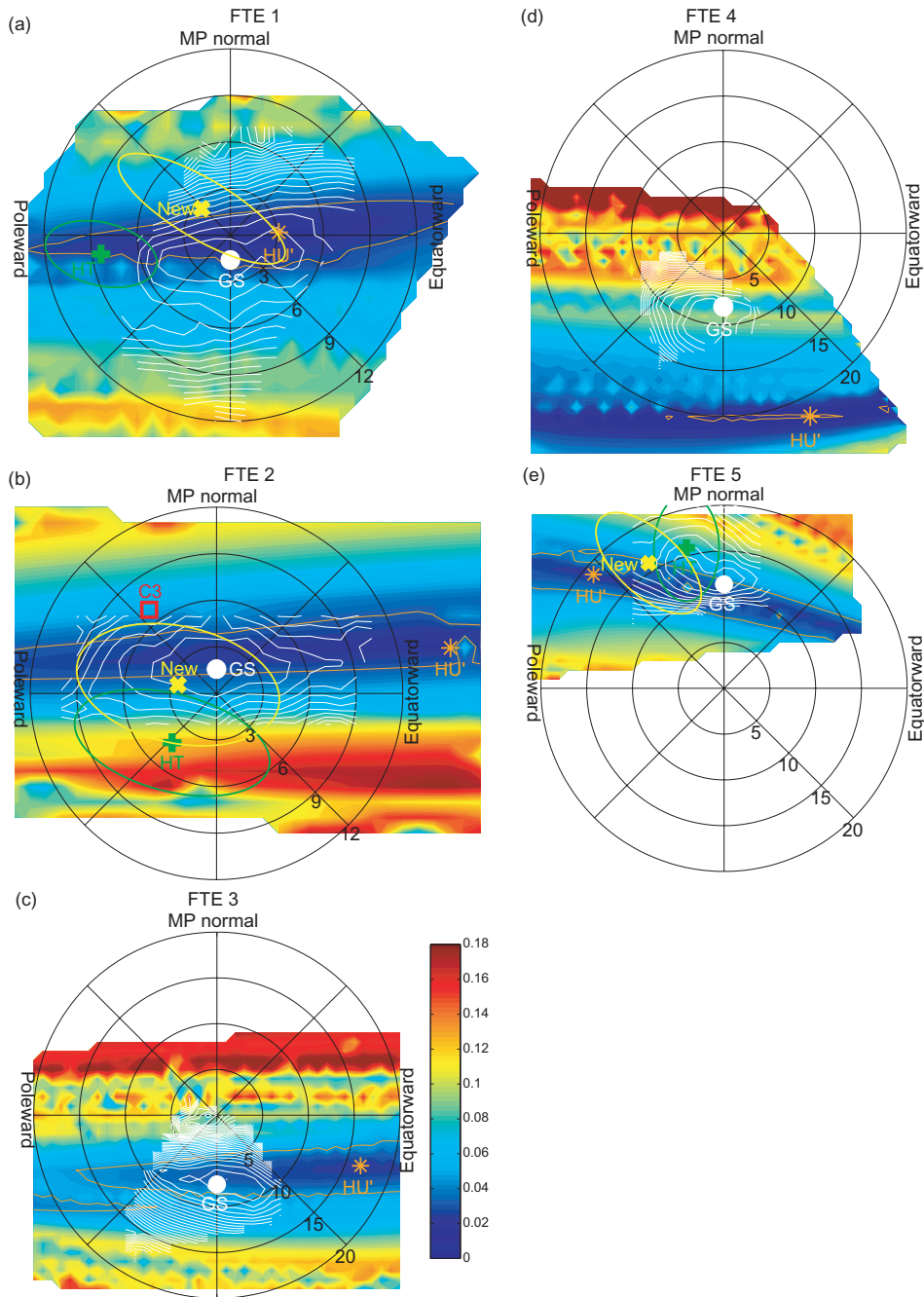
Fig. 9. Polar plots of axis directions for the five FTEs. The bull's-eye represents the vector $\boldsymbol{n}\times(\boldsymbol{k}\times\boldsymbol{n})$, where $\boldsymbol{n}$ is the magnetopause normal determined from MVAB(C) and $\boldsymbol{k}$ is the orientation of the invariant axis from optimal GS reconstruction. In each plot, the magnetopause normal vector is directed upward along the vertical axis. The $\boldsymbol{k}$ axis is denoted by a white dot. By definition, it falls on the vertical axis but coincides with the bull's-eye only when it is strictly perpendicular to the normal vector. White contour lines surrounding the white dot are curves on which the correlation coefficient between the predicted and measured field components (as shown in the bottom panel of Fig. 3) is equal. The background color shows the residue map associated with the fitting of $B_z(A)$ in Fig. 2, as defined by Eq. (5) in Hu and Sonnerup (2002), the orange asterisk represents the axis direction for which the residue has a minimum, and the orange line the directions in which the residue reaches two times the minimum. For FTEs 1, 2, and 5, the axis from a new method for axis determination (Sonnerup and Hasegawa, 2005) is shown by the yellow cross and the axis from MVA of the leftover electric field in the HT frame by the green plus sign. The red open square marks the axis derived by applying the remote sensing method (Khrabrov and Sonnerup, 1998b) to C3 data of FTE 2. Statistical error ellipses are from Eq. (8.23) in Sonnerup and Scheible (1998). A simpler version of the figure was presented for FTEs 1 and 2 by Sonnerup and Hasegawa (2005).

Table 1. Parameters for reconstructed FTEs seen by Cluster on 8 March 2003.

	FTE 1	FTE 2	FTE 3
8 March 2003	(07:02:37–07:03:46 UT)	(07:07:18–07:08:23 UT)	(07:10:42–07:11:56 UT)
GSE components of optimal GS axes			
x	(0.6692, −0.7069, −0.2290)	(0.7338, −0.5896, −0.3375)	(0.6339, −0.2678, −0.4517)
y	(0.5729, 0.2946, 0.7648)	(0.5940, 0.3158, 0.7399)	(0.6406, 0.0991, 0.7614)
z	(−0.4732, −0.6430, 0.6021)	(−0.3296, −0.7434, 0.5820)	(−0.4333, −0.7720, 0.4650)
B_t in rope [Tm]	0.0450	0.0518	0.0268
Rec. E-field [mV m^{-1}]	0.150	0.173	0.112
Reconnection rate	0.041	0.058	0.038
$B_z A$ [MWeber]	1.05	1.96	N/A
$J_z A$ [MA]	−0.39	−0.64	N/A
V_{HT} [km s^{-1}]	(−256, 62, 168)	(−234, 51, 166)	(−249, 35, 205)
$|V_{HT\perp}|$ [km s^{-1}]	254	258	273
cc$_{HT}$	0.976	0.938	0.976
Walén slope	−0.09	−0.16	−0.08
B_{sheath} [nT]	(7.4, −23.3, −2.9)		
B_{sphere} [nT]	(−32.5, 6.1, 22.4)		
Magnetic shear [deg.]	117		

B_t in rope: Total transverse magnetic flux inside the flux rope.
Rec. E-field: Average reconnection electric field at the time of the creation of FTE, calculated by dividing the total reconnected flux (B_t in rope) by the occurrence period of FTEs (4 or 5 min).
$B_z A$: Total axial magnetic flux inside the flux rope; $J_z A$: Total axial current inside the flux rope.

data point was available, i.e. when the structure is in a precise magnetohydrostatic equilibrium and when the axis has a right orientation, while it becomes unity when the average residue is equal to the difference between the maximum and minimum of the measured B_z values. The figure shows that the domain where the residue is small is strongly elongated in the direction perpendicular to the magnetopause normal, with the elongation being consistent with the result of Hu and Sonnerup (2002). We also see that this domain roughly overlaps with that of high correlation coefficients (white contour lines), except for FTE 4. Note that the elongation is much larger than that of the white contour lines, indicating a larger uncertainty for the axis rotation about the normal. Therefore, it is concluded that the present multi-spacecraft (optimal GS based) axis determination is better than the single-spacecraft one. But the single-spacecraft method may be used as a guideline in the search for the optimal GS axis. For FTE 4, in which reconnection activity appears to have been present, the high-correlation domain and small-residue domain are totally separated from each other, contrary to the other four FTEs. It appears that, when field-aligned flows and hence inertia effects are significant, the Hu and Sonnerup method, which is based on the assumption of a precise magnetohydrostatic equilibrium, becomes a poor guideline.

For FTEs 1, 2, and 5, certain other single-spacecraft methods worked fairly well: the results are superposed in Fig. 9. The yellow cross and green plus represent the axis directions calculated from a new method for axis determination (Sonnerup and Hasegawa, 2005), and from the related method of MVA of leftover electric fields in the HT frame. These fields are identically zero, and the methods fail, when a perfect HT frame exists. In reality, there are almost always leftover fields that may exhibit fluctuations which are highly anisotropic with the direction of minimum variance close to the axial direction (see Sonnerup and Hasegawa, 2005, for details). These two methods gave poor results (not shown) for FTEs 3 and 4. Ellipses in the polar plots represent estimates of purely statistical errors from the formulas given by Sonnerup and Scheible (1998). For FTE 2, we also show the axis obtained from "remote sensing" of the FTE by C3 (Khrabrov and Sonnerup, 1998b). For FTEs 1 and 3, the field perturbations at C3 were too small for the remote-sensing method to work successfully. On the other hand, for FTEs 4 and 5, the perturbations were too large to come from remote sensing of the FTE. The remote sensing result (point "C3" in Fig. 9b) is remarkably close to the GS and the "New Method" results, given that the methods from which the orientation was determined are totally different: the remote sensing method uses only magnetic field data from a single spacecraft; the "New

Table 2. Parameters for reconstructed FTEs seen by Cluster on 26 January 2003.

	FTE 4	FTE 5
26 January 2003	(20:53:03–20:53:56 UT)	(20:57:00–20:57:57 UT)
	GSE components of optimal GS axes	
x	(0.7555, 0.2119, −0.6200)	(0.7416, 0.1696, −0.6490)
y	(0.5146, 0.3937, 0.7617)	(0.5635, 0.3673, 0.7399)
z	(0.4055, −0.8945, 0.1884)	(0.3639, −0.9145, 0.1768)
B_t in rope [Tm]	0.0619	0.0621
Rec. E-field [mV m^{-1}]	0.258	0.259
Reconnection rate	0.070	0.074
$B_z A$ [MWeber]	−1.92	−3.59
$J_z A$ [MA]	−0.63	−0.70
V_{HT} [km s^{-1}]	(−387, −12, 268)	(−377, 94, 240)
$|V_{HT\perp}|$ [km s^{-1}]	461	419
cc_{HT}	0.970	0.974
Walén slope	0.39	0.12
B_{sheath} [nT]	(6.7, 19.4, −16.6)	
B_{sphere} [nT]	(−12.5, −13.5, 21.2)	
Magnetic shear [deg.]	160	

Method" uses velocity and magnetic data; and GS uses four-spacecraft measurements.

On the whole, it is seen that the axes from the various methods are mostly clustered within a fairly small area, and are embedded in an elongated domain in which the residue values are small. Importantly, they have a small angle with respect to the GS axis and thus can be used for an initial estimate of the flux rope axis.

In Tables 1 and 2, we summarize important parameters obtained for each FTE. Note that the axis orientation is similar among the events that occurred on the same day, indicating that the observed flux ropes were elongated in a similar direction. The axis bisects the angle (117°) between the magnetosheath and magnetospheric magnetic field directions for FTEs 1–3; it is between the two directions, which in this event form an angle of 160°, but somewhat closer to the magnetosheath field for FTEs 4 and 5. The strong core field seen in the maps appears to indicate that all five FTEs resulted from component merging, because the core field would have its origin in the guide-field present at the reconnection site that created the FTEs. During the period of migration from the reconnection site to the Cluster location, the reconnected flux tube might have been stretched in the axial direction or its radius might have expanded/contracted (Sonnerup et al., 2004), but neither of these can produce a core field without nonzero guide field. Antiparallel merging, therefore, could not have been responsible for the FTEs.

Assuming that the orientation of the flux rope axis represents that of the X-lines which led to the FTEs, then FTEs 4 and 5 do not seem to have originated from subsolar reconnection, while the axes, motion, and observed location of FTEs 1–3 are all consistent with the subsolar merging model. Since the magnetosheath field had a southward and duskward component (see Table 2) when FTEs 4 and 5 were encountered, an X-line formed at the subsolar point would have been tilted northward on the dusk side. But the invariant axis is instead tilted southward on the duskward side of the spacecraft. Thus, the axes for FTEs 4 and 5 are inconsistent, with a particular type of component merging model, which predicts a tilted X-line hinged at the subsolar point in the presence of significant IMF B_y (e.g. Gonzalez and Mozer, 1974; Sonnerup, 1974). However, one should consider the possibility that the orientation of the flux rope axis may be different from that of the X-line responsible for its formation. Such is the case at the two ends of the segment of a flux tube embedded in the magnetopause, where the tube connects to the ionosphere or to the magnetosheath. Since the axis for FTEs 4 and 5 is closer to the magnetosheath field direction, it may be that Cluster encountered the part of the total flux tube that connected to the magnetosheath. If this magnetosheath part was located on the dawnward side of the magnetopause-embedded segment, as expected in the Russell-Elphic model for the Northern Hemisphere under the observed magnetosheath field condition, the reconnection site cannot have been at the subsolar region but would have been located considerably duskward of the noon-midnight

meridian. The reason is that Cluster was on the dusk side and the motion of FTEs 4 and 5 in the y direction was not significant (see the HT velocity components in Table 2).

Tables 1 and 2 also contain information about the minimum values of the reconnection electric field and the reconnection rate, required to create the FTEs. The electric field, intrinsic to reconnection, is computed by dividing the total transverse magnetic flux within the flux rope by the FTE occurrence period of 4 or 5 min, the assumption being that the magnetic flux has been reconnected during the period at a constant reconnection rate. It ranges from $0.112 \, \text{mV m}^{-1}$ (FTE 3) to $0.259 \, \text{mV m}^{-1}$ (FTE 5). The reconnection rate is then computed via the equation: reconnection rate=(reconnection electric field)/($V_{A \, \text{sheath}} B_{\text{sheath}}$), where $V_{A \, \text{sheath}}$ and B_{sheath} are the local magnetosheath Alfvén velocity and magnetic field, based on the components perpendicular to the flux rope axis. It ranges from 0.038 (FTE3) to 0.074 (FTE5). Since the magnetosheath field magnitude near the reconnection site, which must have been at lower latitudes, or possibly even in the Southern Hemisphere, could have been stronger than the local field magnitude, it may well be that our lower bound on the actual reconnection rate could be somewhat smaller than the above values.

6 Summary and discussion

Optimal Grad-Shafranov reconstruction, a technique to generate a 2-D map of plasma and magnetic field structures using multi-spacecraft data, has been applied to five FTEs encountered by Cluster near the northern cusp. The results from our study are summarized as follows.

1. The reconstructed FTEs consist of one or more magnetic flux ropes. Under the assumption that the orientation of the flux rope axis is roughly the same as that of X-line(s), which led to the FTEs, the result indicates the existence of an X-line, both poleward and equatorward of the flux rope. Thus, it is suggested that two or more X-lines were involved in the formation of the observed FTEs, although these X-lines may not have been active simultaneously. All the FTEs were moving antisunward and poleward, indicating that the reconnection which led to the FTEs occurred equatorward of Cluster. For FTEs 1–3, which occurred on 8 March 2003, it is inferred from the absence of reconnection activity (small Walén slopes) and high correlation between the measured and predicted fields (satisfaction of the model assumptions) that the reconnection site was far from the Cluster location and that the FTE flux ropes had reached an approximate, but not complete, equilibrium by the time Cluster encountered them. On the other hand, flows associated with reconnection were observed in or near the FTEs on 26 January 2003 (Fig. 6), in particular in FTE 4 for which the Walén slope was significantly positive. This may indicate that Cluster

was relatively close to an X-line for FTEs 4 and 5. The repetitive occurrence of the FTEs and the presence of multiple flux ropes seen in our data seem consistent with what has recently been found in a global MHD simulation model by J. Raeder. We are not in a position to claim that all FTEs are flux ropes created by multiple X-line reconnection. We have found other FTEs which could not be reconstructed by the GS method and thus appear to have involved significant time evolution or three-dimensionality of the structures. There is a possibility that the GS reconstruction works better for flux rope-type FTEs, which may have a more stable structure. Note that multiple flux ropes have also been found in the solar wind (e.g. Hu et al., 2003) and that near-periodic occurrence of travelling compression regions in the magnetotail, suggestive of multiple X-lines, has been reported (Slavin et al., 2005).

2. The orientation of the flux rope axis can be determined more precisely through optimization of a composite GS map, which uses data from all four spacecraft, than by use of single-spacecraft methods. However, the result from single-spacecraft methods can sometimes be used as a first estimate of the axis orientation. In this manner the trial-and-error search for the optimal GS axis can be focussed to a smaller set of directions. Thanks to the accurate axis determination from optimal GS reconstruction, we have demonstrated that all five FTE flux ropes had strong core fields, which indicates that component merging must have been responsible for their generation. FTEs which occurred on the same day have similar axis orientations. The axis orientation for FTEs 1–3 bisects the angle between the magnetosheath and magnetospheric fields, while that for FTEs 4 and 5 is closer to the magnetosheath field direction. If one postulates that the orientation of the flux rope axis is more or less the same as that of the X-lines which led to the FTEs, the axes for FTEs 1–3 are consistent, but those for FTEs 4 and 5 are inconsistent with a particular type of component merging model which predicts a subsolar X-line that tilts counterclockwise/clockwise, when seen from the Sun, for positive/negative IMF B_y. For FTEs 1–3, the location of the reconnection site inferred from the motion and observed location of the FTEs is also consistent with the subsolar reconnection. For FTEs 4 and 5, on the other hand, a possibility is that the local axis orientation found from the optimal GS method did not coincide with the X-line orientation but that Cluster encountered a portion of the flux tube that was connecting to the magnetosheath field.

3. A lower bound on the average reconnection electric field needed to produce the flux rope can be estimated from the transverse magnetic flux contained within the flux rope and the quasi-periodicity of the FTE occurrence. As seen in Tables 1 and 2, the total magnetic flux ranges

from 0.0268 to 0.0621 Tm. The axial electric field, intrinsic to reconnection, at the time when the FTEs were created, is then calculated by dividing the total flux by the FTE occurrence period of 4–5 min, the result being 0.112 to 0.259 mV m^{-1} (Tables 1 and 2). These values can be converted to the reconnection rate of 0.038 to 0.074, with the values being consistent with those reported in literature (≤ 0.1). As seen in Tables 1 and 2, the reconnection rate was higher for FTEs 4 and 5 which occurred on 26 January 2003 when the local magnetic shear across the magnetopause was higher (160°) than it was for FTEs 1–3 which occurred on 8 March 2003, when the shear was lower (117°).

4. The structure of the observed FTEs has been described reasonably well by the 2-D model. The length of the flux ropes having a 2-D aspect is estimated to have been at least a few R_E, because the spacecraft separation was of the order of 1 R_E and the FTEs moved $\sim 2\,R_E$ along the flux rope axis during the interval (~ 1 min) of the event (the component of the plasma velocity along the axis was about 170 km s^{-1}). Under the assumption that the length of the 2-D segment of the flux ropes is about the same as that of the X-lines, the X-lines associated with the FTEs would have had a length of at least a few R_E.

5. All five FTEs were observed in the Northern Hemisphere during winter/early spring. This fact is consistent with a recent Raeder prediction, based on global numerical simulation, according to which, during strongly southward IMF, FTEs are expected in the Northern, but not Southern Hemisphere during winter. FTEs 4 and 5 satisfy these simulation conditions quite well; FTEs 1–3 not as well. However, we have not examined whether FTEs were in fact absent in the Southern Hemisphere during the winter of 2003.

6. The bulge of the flux rope tends to be larger on the magnetosheath side than on the magnetospheric side. The result is consistent with 2-D MHD simulations (e.g. Scholer, 1989), showing that the FTE signatures become more/less pronounced on the magnetosheath/magnetosphere side of the boundary as the ratio of the magnetosheath to magnetosphere field strength decreases. In general, it is expected that the field perturbation amplitude of FTEs is larger in the magnetosheath than in the magnetosphere. Unless caution is exercised, this effect may skew occurrence statistics to show more FTE events in the magnetosheath than in the magnetosphere.

References

Balogh, A., Carr, C. M., Acuña, M. H., et al.: The Cluster magnetic field investigation: Overview of in-flight performance and initial results, Ann. Geophys., 19, 1207–1217, 2001,
SRef-ID: 1432-0576/ag/2001-19-1207.

Cowley, S. W. H.: The causes of the convection in the Earth's magnetosphere: A review of developments during IMS, Rev. Geophys., 20, 531–565, 1982.

Farrugia, C. J., Southwood, D. J., Cowley, S. W. H., Rijnbeek, R. P., and Daly, P. W.: Two-regime flux transfer events, Planet. Space Sci., 35, 737–744, 1987.

Gonzalez, W. D. and Mozer, F. S.: A quantitative model for the potential resulting from reconnection with an arbitrary interplanetary magnetic field, J. Geophys. Res., 79, 4186–4194, 1974.

Gustafsson, G., André, M., Carozzi, T., et al.: First results of electric field and density observations by Cluster EFW based on initial months of operation, Ann. Geophys., 19, 1219–1240, 2001,
SRef-ID: 1432-0576/ag/2001-19-1219.

Haerendel, G., Paschmann, G., Sckopke, N., Rosenbauer, H., and Hedgecock, P. C.: The front-side boundary layer of the magnetosphere and the problem of reconnection, J. Geophys. Res., 83, 3195–3216, 1978.

Hasegawa, H., Sonnerup, B. U. Ö., Dunlop, M. W., Balogh, A., Haaland, S. E., Klecker, B., Paschmann, G., Lavraud, B., Dandouras, I., and Rème, H.: Reconstruction of two-dimensional magnetopause structures from Cluster observations: Verification of method, Ann. Geophys., 22, 1251–1266, 2004,
SRef-ID: 1432-0576/ag/2004-22-1251.

Hasegawa, H., Sonnerup, B. U. Ö., Klecker, B., Paschmann, G., Dunlop, M. W., and Rème, H.: Optimal reconstruction of magnetopause structures from Cluster data, Ann. Geophys., 23, 973–982, 2005,
SRef-ID: 1432-0576/ag/2005-23-973.

Hau, L.-N. and Sonnerup, B. U. Ö.: Two-dimensional coherent structures in the magnetopause: Recovery of static equilibria from single-spacecraft data, J. Geophys. Res., 104, 6899–6917, 1999.

Hu, Q. and Sonnerup, B. U. Ö.: Magnetopause transects from two spacecraft: A comparison, Geophys. Res. Lett., 27, 1443–1446, 2000.

Hu, Q. and Sonnerup, B. U. Ö.: Reconstruction of magnetic flux ropes in the solar wind, Geophys. Res. Lett., 28, 467–470, 2001.

Hu, Q. and Sonnerup, B. U. Ö.: Reconstruction of magnetic clouds in the solar wind: Orientation and configuration, J. Geophys. Res., 107(A7), 1142, doi:10.1029/2001JA000293, 2002.

Hu, Q. and Sonnerup, B. U. Ö.: Reconstruction of two-dimensional structures in the magnetopause: Method improvements, J. Geophys. Res., 108(A1), 1011, doi:10.1029/2002JA009323, 2003.

Hu, Q., Smith, C. W., Ness, N. F., and Skoug, R. M.: Double flux-rope magnetic cloud in the solar wind at 1 AU, Geophys. Res. Lett., 30(7), 1385, doi:10.1029/2002GL016653, 2003.

Khrabrov, A. V. and Sonnerup, B. U. Ö.: DeHoffmann-Teller analysis, in: Analysis Methods for Multi-Spacecraft Data, ISSI Sci. Rep., SR-001, Kluwer Acad., Norwell, Mass., 221–248, 1998.

Khrabrov, A. V. and Sonnerup, B. U. Ö.: Magnetic variance analysis for small-amplitude waves and flux transfer events on a current sheet, J. Geophys. Res., 103, 11 907–11 918, 1998.

Lee, L. C. and Fu, Z. F.: A theory of magnetic flux transfer at the Earth's magnetopause, Geophys. Res. Lett., 12, 105–108, 1985.

Raeder, J.: Flux transfer events: 1. Generation mechanism for nearly southward IMF, Ann. Geophys., 24, 381–392, 2006.

Rème, H., Aoustin, C., Bosqued, J. M., et al.: First multispacecraft ion measurements in and near the Earth's magnetosphere with the identical Cluster ion spectrometry (CIS) experiment, Ann. Geophys., 19, 1303–1354, 2001,
SRef-ID: 1432-0576/ag/2001-19-1303.

Rijnbeek, R. P., Cowley, S. W. H., Southwood, D. J., and Russell, C. T.: A survey of dayside flux transfer events observed by ISEE 1 and 2 magnetometers, J. Geophys. Res., 89, 786–800, 1984.

Russell, C. T. and Elphic, R. C.: Initial ISEE magnetometer results: Magnetopause observations, Space Sci. Rev., 22, 681–715, 1978.

Saunders, M. A., Russell, C. T., and Sckopke, N.: Flux transfer events, scale size and interior structure, Geophys. Res. Lett., 11, 131–134, 1984.

Scholer, M.: Magnetic flux transfer at the magnetopause based on single X-line bursty reconnection, Geophys. Res. Lett., 15, 291–245, 1988.

Scholer, M.: Asymmetric time-dependent and stationary magnetic reconnection at the dayside magnetopause, J. Geophys. Res., 94, 15 099–15 111, 1989.

Sibeck, D. G.: A model for the transient magnetospheric response to sudden solar wind dynamic pressure variations, J. Geophys. Res., 95(A4), 3755–3771, 1990.

Slavin, J. A., Tanskanen, E. I., Hesse, M., Owen, C. J., Dunlop, M. W., Imber, S., Lucek, E. A., Balogh, A., and Glassmeier, K.-H.: Cluster observations of traveling compression regions in the near-tail, J. Geophys. Res., 110, A06207, doi:10.1029/2004JA010878, 2005.

Sonnerup, B. U. Ö.: Magnetopause reconnection rate, J. Geophys. Res., 79, 1546–1549, 1974.

Sonnerup, B. U. Ö. and Guo, M.: Magnetopause transects, Geophys. Res. Lett., 23, 3679–3682, 1996.

Sonnerup, B. U. Ö. and Scheible, M.: Minimum and maximum variance analysis, in: Analysis Methods for Multi-Spacecraft Data, ISSI Sci. Rep., SR-001, Kluwer Acad., Norwell, Mass., 185–220, 1998.

Sonnerup, B. U. Ö., Hasegawa, H., and Paschmann, G.: Anatomy of a flux transfer event seen by Cluster, Geophys. Res. Lett., 31, L11803, doi:10.1029/2004GL020134, 2004.

Sonnerup, B. U. Ö. and Hasegawa, H.: Orientation and motion of two-dimensional structures in a space plasma, J. Geophys. Res., 110, A06208, doi:10.1029/2004JA010853, 2005.

Southwood, D. J., Farrugia, C. J., and Saunders, M. A.: What are flux transfer events?, Planet. Space Sci., 36, 503–508, 1988.

Walthour, D. W., Sonnerup, B. U. Ö., Paschmann, G., Lühr, H., Klumpar, D., and Potemra, T.: Remote sensing of two-dimensional magnetopause structures, J. Geophys. Res., 98, 1489–1504, 1993.

Walthour, D. W., Sonnerup, B. U. Ö., Elphic, R. C., and Russell, C. T.: Double vision: Remote sensing of a flux transfer event with ISEE 1 and 2, J. Geophys. Res., 99, 8555–8563, 1994.